Transient Studies and Kinetic Modeling of Ethylene Oxidation on Pt/SiO_2

This paper describes a reaction-reactor model, utilizing alternative reaction pathways, developed to explain experimental results from the total oxidation of ethylene on a Pt/SiO_2 catalyst. Transient temperature-programmed reaction and concentration-programmed reaction experiments were utilized to study the reaction through FTIR spectroscopic and surface temperature measurements combined with bulk measurements of concentration and temperature. Different elementary-step pathways were incorporated into the concentration and energy balances in performing the simulations. One pathway utilized adsorbed CO, formed from adsorbed ethylene, as the route to CO_2 formation. This pathway is shown to become important under ethylene-rich conditions. The second pathway utilized the direct reaction between adsorbed ethylene and adsorbed oxygen as the path to CO_2 formation. The latter route is shown to become important under oxygen-rich conditions. Finally, an example is utilized to show the advantages of the nonequilibrium elementary-step modeling approach over conventional "equilibrium" models where only one step is taken to be rate-determining.

Ravindra Sant
David J. Kaul
Eduardo E. Wolf
Department of Chemical Engineering
University of Notre Dame
Notre Dame, IN 46556

Introduction

The oxidation of light hydrocarbons on Pt has received considerable attention in recent years due to the use of platinum catalysts in catalytic converters to control automotive exhaust emissions. Among these reactions, perhaps the most widely-studied has been the oxidation of ethylene. These studies have been performed at atmospheric pressures on supported Pt (e.g., in fixed beds) and also at ultrahigh vacuum (UHV) conditions on single crystals of Pt.

Packed-bed, flow-through and recycle reactor studies of ethylene oxidation have been reported by several researchers on silica- or alumina-supported Pt. The rate of formation of CO_2 has been reported by some to exhibit a negative-order dependence on ethylene and a positive-order dependence on oxygen (Cant and Hall, 1970; Hawkins and Wanke, 1979). Others have concluded that the rate dependencies are different for excess ethylene than for conditions involving excess oxygen (Vayenas et al., 1980, 1981). There have been suggestions that different rate-determining steps are involved in these two situations (Carberry, 1977). Thus far, however, models have usually involved global rate expressions, which were not based on the underlying chemistry.

At UHV conditions, the interaction of ethylene with single crystal and polycrystalline surfaces of Pt in the presence and in the absence of oxygen has been the subject of much recent work (Palmer, 1975; Fischer and Kelemen, 1977; Steininger et al., 1982; Berlowitz et al., 1985; Wang et al., 1985; Beebe and Yates, 1987). Here, the focus has been primarily on (i) the nature of the species into which ethylene is converted after being adsorbed on Pt, and (ii) the sequence of reactions between coadsorbed ethylene and oxygen leading to the formation of CO_2 and water. Briefly, in the absence of oxygen, adsorbed ethylene is reported to be rehybridized and converted to ethylidyne (Steininger et al., 1982; Berlowitz et al., 1985; Wang et al., 1985; Beebe and Yates, 1987), and also to be dehydrogenated to varying degrees (Palmer, 1975; Fischer and Kelemen, 1977). In the presence of adsorbed oxygen, adsorbed ethylene is said to be converted to CO_2 and water via a surface acetylenic species (Palmer, 1975; Bertlowitz et al., 1985). Some researchers have reported finding no evidence for carboxyl- or hydroxyl-containing intermediates (Steininger et al., 1982).

Correspondence concerning this paper should be addressed to E. E. Wolf.
Present address of D. J. Kaul: Cabot Corp. Research Labs., Boston, MA 01821.

The present work describes the development of a reaction-reactor model for the oxidation of ethylene on Pt/SiO_2, which considers two alternative reaction pathways leading to CO_2 formation. The objectives of this work were threefold:

1. To explain the observed experimental behavior in terms of the reaction processes occurring on the catalyst surface and the interactions between transport processes and the reaction kinetics
2. To examine whether these surface reaction processes could be described realistically via the reaction of adsorbed oxygen with adsorbed ethylene and with intermediates derived from adsorbed ethylene
3. To examine conditions under which one of the adsorbed intermediates might be adsorbed CO, as a pathway to the formation of CO_2

The experiments involve transient FTIR studies over a wide range of operating conditions and have been described by Kaul and Wolf (1986); they will be considered in some detail in the experimental section. The reaction models considered are each based on a sequence of elementary steps developed from several UHV studies reported in the literature. The first model utilizes adsorbed CO, formed as a decomposition product from adsorbed ethylene, as the reaction intermediate leading to the formation of CO_2. The second model utilizes the direct reaction of adsorbed ethylene with adsorbed oxygen as the route to CO_2 production. The surface science results were combined with our infrared studies to integrate the surface chemistry with results on supported catalysts. The strategy used in relating the modeling effort to the experimental results was the construction of the experimental and simulated cross-sections of the bifurcation set. The bifurcation set shows how regions of unique and multiple steady states change with the inlet concentrations of the reactants and with the reactor temperature.

Experimental

Experiments were performed in a small volume (6×10^{-6} m^3) infrared cell reactor. A brief outline of the reactor system is presented here, and a detailed description is available elsewhere (Kaul and Wolf, 1984). A wafer of the silica-supported catalyst (about 1.0×10^{-5} m thick and about 0.019 m in diameter) is held between two stainless steel flanges which form the body of the reactor. Gases flow into and out of the reactor on either side of the wafer, and openings in the catalyst holder (which also serves as the gasket) promote mixing between the regions on either side of the wafer. CaF_2 windows fitted in the center of each flange permit the passage of the infrared beam, and four foil thermocouples in direct contact with the catalyst wafer provide a sensitive measurement of what we consider the local catalyst surface temperature. Two of these thermocouples are located on either side of the wafer, the thermocouples on one side being diagonally opposite each other. Taken together, both sides of a 0.01 m^2 region are sampled.

Programmable mass flow and temperature controllers were used to carry out experiments in one of two ways: either by programming the flow rate of one of the reactants to increase and decrease linearly with all other inputs being held constant [a concentration-programmed reaction (CPR) experiment] or by programming the reactor wall temperature to increase and decrease quasilinearly [a temperature-programmed reaction (TPR) experiment] while all flow rates were kept constant. For example, at any time when an oscillatory state was attained, the programmed variable was also held constant. The reactor is placed in the sample chamber of a Digilab FTS-15C FTIR spectrometer which permits continuous monitoring of adsorbed and gas-phase species. The exit gas stream is continuously monitored for the concentrations of CO and CO_2 via on-line Beckman infrared analyzers.

Two series of 5 wt. % Pt/SiO_2 catalysts were used, each prepared by the incipient wetness method. After vacuum-drying at room temperature for 24 h, the catalyst was calcined for 6 h at 300°C and then reduced for 12 h at 200°C. Chemisorption measurements indicated a dispersion of 16.9% for one catalyst batch, to be denoted as catalyst A, and 14.3% for the other catalyst batch, to be denoted as catalyst B.

Figure 1 shows the results of a typical TPR experiment. It was performed at 1% ethylene, 11% oxygen, and 180 cm^3/min nitrogen. The lower curve in Figure 1a shows the reactor temperature as it was ramped first up and then down in a quasi-linear fashion. The dashed lines in Figure 1a show the response of the catalyst surface temperature at the inlet side and at the exit side. The surface temperature is initially (in the low conversion state) close to the reactor temperature, but after ignition the surface temperature is significantly higher. The rapid rise in the rate of CO_2 production, after ignition, can be observed in Figure 1b where the dashed lines denote the experimental results. Once in the high conversion state, the wall temperature was lowered until extinction occurred, resulting in a drop in sur-

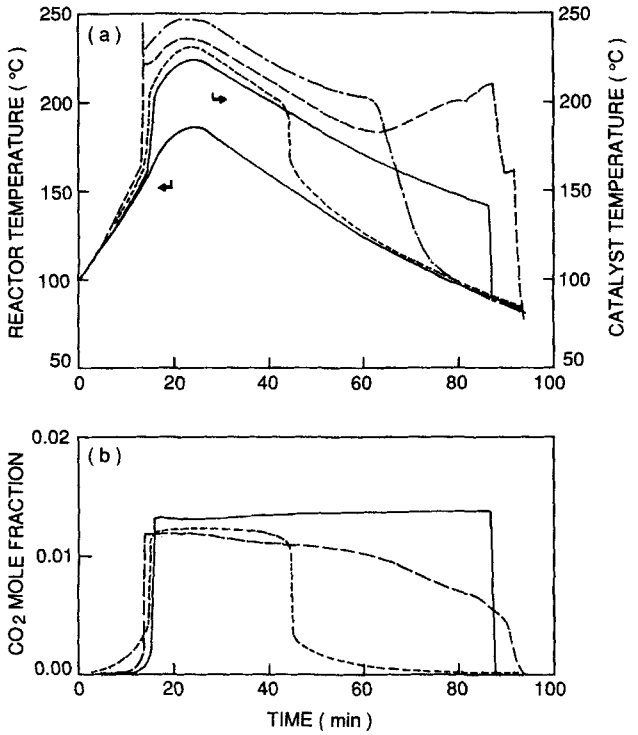

Figure 1. Experimental and simulated results of a TPR experiment at 2.1 cm^3/min ethylene, 23 cm^3/min oxygen, and 180 cm^3/min nitrogen.

(a) Response of the catalyst surface temperature; (b) CO_2 production rate. In (a) and (b): - - - Model 1; —— Model 2. In (a): —·— inlet-side (experimental); ——— exit-side (experimental). In (b): ——— experiment.

face temperature and in CO_2 production. It can be noted that the inlet side and the exit side do not extinguish at the same time. This is just one example of spatial nonuniformities during this reaction. Kaul and Wolf (1986) have described a variety of spatially nonuniform rates and temperatures during oscillatory and transient behavior for this reaction system. The steady-state portion of any experiment, however, displayed spatially uniform behavior. For this reason as well as for ease of computational work, the present model is a spatially uniform one, and it is intended to model mainly the steady-state portion of the experiments.

Theory

Previous work on the Pt-catalyzed oxidation of CO has shown how nonequilibrium elementary-step kinetics and overall mass and energy balances can be combined to simulate the steady state, ignition, extinction and hysteresis behavior observed experimentally (Kaul et al., 1987). The present work utilized a similar approach to simulate steady-state multiplicity for the oxidation of ethylene on Pt. The Pt-catalyzed oxidation of ethylene was assumed to occur through elementary steps involving the adsorption and desorption of ethylene and oxygen, the decomposition and desorption of intermediates formed from adsorbed ethylene, and the surface reaction between adsorbed oxygen and dehydrogenated intermediates from adsorbed ethylene. The first (more general) model considered adsorbed CO as the intermediate leading from adsorbed ethylene to CO_2 production. The behavior of adsorbed CO (subsequent to its formation from adsorbed ethylene) was described by identical processes and rate constants to those used earlier by us while modeling CO oxidation on Pt/SiO_2 (Kaul et al., 1987). The second (more specific) model considered the intermediates to be lumped together with adsorbed ethylene and utilized the direct surface reaction between adsorbed ethylene and adsorbed oxygen as the means for CO_2 formation.

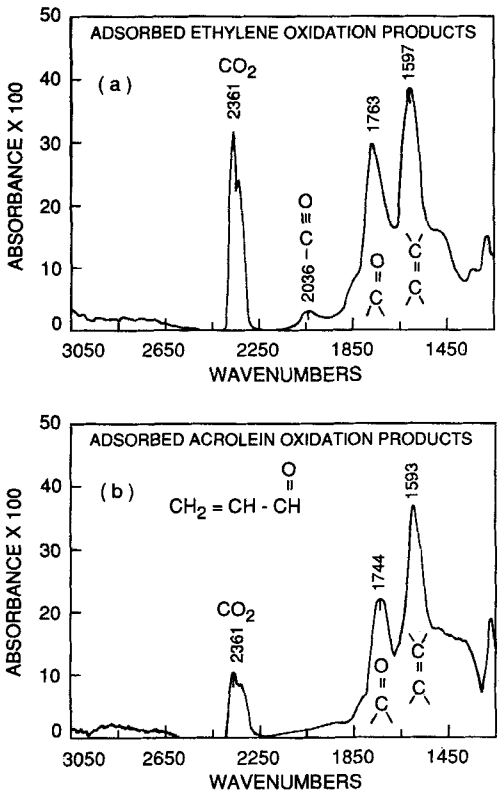

Figure 2. Infrared spectra of partial oxidation products on Pt/SiO_2 at 150°C during (a) ethylene oxidation and (b) acrolein oxidation.

Reactant concentrations: oxygen, 9%; ethylene/acrolein, 6%; balance nitrogen. Conversion of oxygen (limiting reactant): 30%.

Reaction pathways

Much debate exists in the literature regarding the sequence of steps by which adsorbed ethylene and adsorbed oxygen react with each other. For example, the extent to which adsorbed ethylene decomposes before reacting is still not known. According to the results of Palmer (1975), adsorbed ethylene is dehydrogenated, first to a surface acetylenic species and then via reaction with adsorbed oxygen to surface carbon. This carbon is then oxidized to CO and finally to CO_2. The studies of Steininger et al. (1982) indicate that, in the presence of coadsorbed oxygen, adsorbed ethylene exists primarily in a di-σ bonded form. The reaction between adsorbed ethylene and adsorbed oxygen results in the formation of CO_2 and water with no evidence for oxygen-containing intermediates. According to these authors, some surface carbon may also be formed, this being oxidized to CO. Kung and coworkers, on the basis of their TPD studies of C_2H_4 on oxygen-covered Pt, have also proposed that adsorbed ethylene is dehydrogenated to an acetylenic species which then reacts with adsorbed oxygen to form CO, CO_2, and water (Berlowitz et al., 1985; Megiris et al., 1985).

Figure 2 shows typical spectra from our studies of infrared features during the oxidation of ethylene and of related compounds on supported Pt. These studies were performed on catalyst A and details can be obtained in Kaul (1985). Briefly, ethylene oxidation under oxygen-lean conditions revealed the presence of adsorbed CO and of bands attributable to >C═O and >C═C< groups among the adsorbed species. This spectrum is shown in Figure 2a. The inference of the presence of a dehydrogenated acrolein-like skeleton was supported by the observation of bands corresponding to >C═O and >C═C< during the oxidation of acrolein on the same catalyst. The latter spectrum is shown in Figure 2b. Furthermore, the oxidation of formic acid and of acetaldehyde (on the same catalyst) revealed the presence of adsorbed CO as well as bands which could be assigned to —C—H and >C═O species.

Temperature-programmed desorption (TPD) studies on oxygen-covered Pt(111) have shown that most of the desorption of ethylene occurs below 250 K (Steininger et al., 1982; Berlowitz et al., 1985). At temperatures higher than 250 K, CO_2, H_2O, H_2, and CO are the main desorption products. Hence, inhibition by ethylene at temperatures of interest in this study (300–600 K) is more likely to result from the decomposition products and reaction intermediates from ethylene than by adsorbed ethylene itself. One of the reaction intermediates could well be adsorbed CO. Other intermediates have also been proposed, e.g., a species denoted as $(CH)_xO_y$ (Berlowitz et al., 1985).

Based on our studies as well as those of the other researchers described here, we outline the following sequence of steps in the

reaction between adsorbed ethylene and adsorbed oxygen on supported Pt:

$$
\begin{array}{rcl}
 & C_2H_4(a) \rightarrow C_2H_2(a) & + 2H(a) \\
C_2H_2(a) + & O(a) \rightarrow C_2H_2O(a) & \\
C_2H_2O(a) + & O(a) \rightarrow C_2HO(a) & + OH(a) \\
C_2HO(a) + & O(a) \rightarrow CO(a) & + OH(a) + C(a) \\
C(a) + & O(a) \rightarrow CO(a) & \\
2 \times [CO(a) + & O(a) \rightarrow CO_2(g)] & \\
2 \times [OH(a) + & H(a) \rightarrow H_2O(g)] & \\
\hline
C_2H_4(a) + & 6O(a) \rightarrow 2CO_2(g) & + 2H_2O(g)
\end{array}
$$

The sequence just described is among the simplest that can be written in terms of elementary steps. Since the rate of formation or reaction of some intermediates is very rapid or not known, and/or their concentrations too low, the conversion of adsorbed ethylene to CO_2 was lumped into two different pathways, denoted as Models 1 and 2. In Model 1, the reaction proceeds as follows:

$$O_2 + 2S \leftrightarrow 2\,O \cdot S$$

$$C_2H_4 + 2S \leftrightarrow C_2H_4 \cdot 2S$$

$$C_2H_4 \cdot 2S + 4\,O \cdot S \rightarrow 2\,CO \cdot S + 2\,H_2O + 4S$$

$$CO \cdot S \leftrightarrow CO + S$$

$$CO \cdot S + O \cdot S \rightarrow CO_2 + 2S$$

whereas, in Model 2, the pathway is represented by the direct reaction between adsorbed ethylene and adsorbed oxygen, i.e.,

$$C_2H_4 + 2S \leftrightarrow C_2H_4 \cdot 2S$$

$$O_2 + 2S \leftrightarrow 2\,O \cdot S$$

$$C_2H_4 \cdot 2S + 6\,O \cdot S \rightarrow 2\,CO_2 + 2\,H_2O + 8\,S$$

These reaction models are incorporated into the adsorption-decomposition-reaction steps and the mass and energy balances to describe the experimental results.

Adsorption-desorption

Oxygen:

$$O_2 + 2S \leftrightarrow 2O \cdot S$$

where S denotes an active site. The terms for the adsorption and desorption of oxygen were unchanged from the expressions and parameters used during CO oxidation on Pt (Kaul et al., 1987). The adsorption and desorption rate constants are shown in Eqs. 1.4 and 1.5 of Table 1. These steps were the same for Models 1 and 2. Theoretically, it has been shown that the factor $(1-\theta_1)^2$ in the denominator of the term for oxygen desorption arises when considering a precursor model for dissociative adsorption-desorption (Gorte and Schmidt, 1978). Experimentally, during both CO-CPR and ethylene-CPR experiments, we have found that CO/ethylene reacts readily with an oxygen-covered surface. The models predict this behavior only by including the $(1-\theta_1)^2$ factor to limit the saturation coverage by oxygen. Also, since

Table 1. Model 1: Assumed Mechanism and Balance Equations

(1) $O_2 + 2S \leftrightarrow 2O \cdot S$
(2) $C_2H_4 + 2S \leftrightarrow C_2H_4 \cdot 2S$
(3) $C_2H_4 \cdot 2S + 4O \cdot S \rightarrow 2CO \cdot S + 2H_2O + 4S$
(4) $CO \cdot S \leftrightarrow CO + S$
(5) $CO \cdot S + O \cdot S \rightarrow CO_2 + 2S$

Surface Balances

(1.1) $(d\theta_1/dt) = 2k_1C_{s,1}(1-\theta_1-\theta_2-\theta_3)^2 - 2k_{-1}[\theta_1/(1-\theta_1)]^2 - 2k_3\theta_1\theta_2 - k_5\theta_1\theta_3$
(1.2) $(d\theta_2/dt) = 2k_2C_{s,2}(1-\theta_1-\theta_2-\theta_3)^2 - 2k_{-2}\theta_2 - k_3\theta_1\theta_2$
(1.3) $(d\theta_3/dt) = k_4C_{s,4}(1-\theta_1-\theta_2-\theta_3) + k_3\theta_1\theta_2 - k_{-4}\theta_3 - k_5\theta_1\theta_3$
(1.4) $k_i = (S_i/N_s)[R_2T_s/(2\pi M_i)]^{0.5} \quad i = 1, 2, 4$
(1.5) $k_{-i} = k_{0,-i}\exp[-E_i/(R_3T_s)] \quad i = 1, 2$
$k_{-4} = k_{0,-4}\exp[-(E_4 - \Omega_4\theta_3)/(R_3T_s)]$
(1.6) $k_i = k_{0,i}\exp[-E_i/R_3T_s)] \quad i = 3, 5$

Subscripts 1, 2, 3, 4, and 5 refer to oxygen, ethylene, CO_2, CO, and water, respectively, except for θ_3, where 3 refers to CO.

Intraphase Balances

(1.7) $\epsilon_s(dC_{s,i}/dt) = (k_g/L)(C_{g,i} - C_{s,i}) - aN_sA_i$
where
$A_1 = k_1C_{s,1}(1-\theta_1-\theta_2-\theta_3)^2 - k_{-1}(\theta_1/(1-\theta_1))^2$
$A_2 = k_2C_{s,2}(1-\theta_1-\theta_2-\theta_3)^2 - k_{-2}\theta_2$
$A_3 = -k_5\theta_1\theta_3$
$A_4 = k_4C_{s,4}(1-\theta_1-\theta_2-\theta_3) - k_{-4}\theta_3$
$A_5 = -k_3\theta_1\theta_2$
(1.8) $V_s\rho_sC_{ps}(dT_s/dt) = V_saN_s\Delta H_5k_3\theta_1\theta_3 + V_saN_s\Delta H_3k_3\theta_1\theta_2 - h_sA_s(T_s - T_g)$

Bulk Gas-Phase Balances

(1.9) $V_r(dC_{g,i}/dt) = Q(C_{in,i} - C_{g,i}) - A_sk_g(C_{g,i} - C_{s,i})$
(1.10) $V_r\rho_gC_{pg}(dT_g/dt) = U_wA_r(T_w - T_g) - Q\rho_gC_{pg}(T_g - T_w) + h_sA_s(T_s - T_g)$

this term is important only for an oxygen-covered surface, the $(1-\theta_1)^2$ term is necessary, rather than $(1-\theta_1-\theta_2)^2$ or $(1-\theta_1-\theta_2-\theta_3)^2$.

Ethylene:

$$C_2H_4 + 2S \leftrightarrow C_2H_4 \cdot 2S$$

The rate of ethylene adsorption was taken to be proportional to the square of the fraction of vacant sites. This assumes that the adsorption of ethylene requires two adjacent vacant sites. This is not unreasonable considering that at low temperatures ethylene is reported to adsorb [on Pt(111)] in a di-σ fashion, this form of ethylene being transformed at room temperature to a species which is proposed to be ethylidene or ethylidyne or a vinyl species (Bertolini and Massardier, 1984). The rate of adsorption of ethylene was also taken to be proportional to the intraphase concentration of ethylene just above the catalyst surface. The adsorption rate constant, k_2, was taken to be the product of the collision number and a coverage-independent sticking coefficient, as shown in Eq. 1.4 of Table 1.

The rate of desorption of ethylene was taken to be proportional to the coverage of adsorbed ethylene with the rate constant being an Arrhenius-type expression. This is shown in Eqs. 1.5 and 2.4 of Tables 1 and 2, respectively.

Carbon monoxide:

$$CO \cdot S \leftrightarrow CO + S$$

In Model 1, the desorption and readsorption of CO was described by the above equation. The adsorption and desorption rate parameters for CO were identical to those we have used previously (Kaul et al., 1987).

Surface reaction

Model 1. The rate of the surface reaction between adsorbed CO (formed from adsorbed ethylene) and adsorbed oxygen was assumed to be proportional to the product of their respective coverages:

$$CO \cdot S + O \cdot S \rightarrow CO_2 + 2S$$

The preexponential factor and activation energy for this reaction were taken from the model developed previously by us for CO oxidation on Pt/SiO_2 (Kaul et al., 1987).

Model 2. The rate of the surface reaction was assumed to be proportional to the product of the coverages of adsorbed ethylene and adsorbed oxygen. The rate constant was taken to be of an Arrhenius type, as shown in Eq. 2.5 of Table 2. In the absence of relevant single crystal data for the surface reaction rate constants, values of the preexponential factor and activation energy were adjusted between the limits of values reported from studies at atmospheric pressure in fixed beds and shown in Table 3.

Balance equations

Balances were written for the different species, as shown in Tables 1 and 2 for Models 1 and 2, respectively. The surface concentration balances are shown as Eqs. 1.1, 2.1 (oxygen), Eqs. 1.2, 2.2 (ethylene), and Eq. 1.3 (CO). The concentration balances for intraphase species are shown as Eqs. 1.7 and 2.6, and for the bulk gas-phase species they are shown as Eqs. 1.9 and 2.8. Energy balances were also written for the intraphase (Eqs. 1.8 and 2.7) and the bulk gas-phase (Eqs. 1.10 and 2.9). All the variables were assumed to be spatially uniform for reasons stated in the experimental section.

In the balance equations, subscripts 1–5 refer to oxygen, ethylene, CO_2, CO, and water, respectively, except where noted otherwise. The surface coverage, θ_i, of any particular species i, is taken to be the ratio of the number of surface Pt atoms occupied by that species, i, to the total number of surface Pt atoms.

The mass transfer coefficient, k_g, and the reactor wall–to–gas heat transfer coefficient, U_w, had the same values as those that

Table 2. Model 2: Assumed Mechanism and Balance Equations

(1) $O_2 + 2S \leftrightarrow 2O \cdot S$
(2) $C_2H_4 + 2S \leftrightarrow C_2H_4 \cdot 2S$
(3) $C_2H_4 \cdot 2S + 6O \cdot S \rightarrow 2CO_2 + 2H_2O + 8S$

Surface Balances

(2.1) $d\theta_1/dt = 2k_1C_{s,1}(1-\theta_1-\theta_2)^2 - 2k_{-1}[\theta_1/(1-\theta_1)]^2 - 3k_3\theta_1\theta_2$
(2.2) $d\theta_2/dt = 2k_2C_{s,2}(1-\theta_1-\theta_2)^2 - 2k_{-2}\theta_2 - k_3\theta_1\theta_2$

where

(2.3) $k_i = S_i[RT_s/(2\pi M_i)]^{1/2}/N_s \quad i = 1, 2$
(2.4) $k_{-i} = k_{0,-i} \exp[-E_i/(RT_s)] \quad i = 1, 2$
(2.5) $k_i = k_{0,i} \exp(-E_i/(RT_s)) \quad i = 3$

Intraphase Balances

(2.6) $\epsilon_s(dC_{s,i}/dt) = (k_g/L)(C_{g,i} - C_{s,i}) - aN_s\{k_iC_{s,i}(1-\theta_1-\theta_2)^2 - k_{-i}A_i\}$

where

$A_1 = [\theta_1/(1-\theta_1)]^2$
$A_2 = \theta_2$
when $i = 3$, the terms within { } are replaced by $-k_i\theta_1\theta_2$

(2.7) $V_s\rho_sC_{ps}(dT_s/dt) = 0.5V_s\Delta H_raN_sk_3(T_s)\theta_1\theta_2 - h_sA_s(T_s - T_g)$

Bulk Gas-Phase Balances

(2.8) $V_r(dC_{g,i}/dt) = Q(C_{in,i} - C_{g,i}) - A_sk_g(C_{g,i} - C_{s,i})$
(2.9) $V_r\rho_gC_{pg}(dT_g/dt) = U_wA_r(T_w - T_g) - Q\rho_gC_{pg}(T_g - T_w) + h_sA_s(T_s - T_g)$

Table 3. Values of Kinetic Parameters

Parameter	Unit	Value	Lit. Value	Reference
Models 1 and 2				
S_1	—	0.01	0.01	Kaul et al. (1987)
$k_{0,-1}$	s^{-1}	2.4×10^{13}	2.4×10^{13}	Kaul et al. (1987)
E_1	J/mol	2.17×10^5	2.17×10^5	Kaul et al. (1987)
S_2	—	0.35	0.2–0.5	Fischer & Kelemen (1977)
Model 1				
$k_{0,-2}$	s^{-1}	1.0×10^{13}	1.0×10^{13}	Berlowitz et al. (1985)
E_2	J/mol	5.73×10^4	5.73×10^4	Berlowitz et al. (1985)
$k_{0,3}$	s^{-1}	6.0×10^{13}	—	—
E_3	J/mol	6.27×10^4	—	—
S_4	—	0.35	0.35	Kaul et al. (1987)
$k_{0,-4}$	s^{-1}	6.5×10^{13}	6.5×10^{13}	Kaul et al. (1987)
E_4	J/mol	1.17×10^5	1.17×10^5	Kaul et al. (1987)
Ω_4	J/mol	2.09×10^4	2.09×10^4	Kaul et al. (1987)
$k_{0,5}$	s^{-1}	2.7×10^6	2.7×10^6	Kaul et al. (1987)
E_5	J/mol	5.43×10^4	5.43×10^4	Kaul et al. (1987)
Model 2				
$k_{0,-2}$	s^{-1}	6.5×10^{13}	1.0×10^{13}	Berlowitz et al. (1985)
E_2	J/mol	1.15×10^5	5.73×10^4	Berlowitz et al. (1985)
$k_{0,3}$	s^{-1}	8.0×10^7	2.1×10^8	Cant & Hall (1970)
E_3	J/mol	5.43×10^4	7.73×10^4	Cant & Hall (1970)

we had used for CO oxidation (Kaul et al., 1987) for the same reactor model. The catalyst surface–to–gas heat transfer coefficient, h_s, had to be increased slightly from the value for the oxidation of CO to account properly for the extinction curve, i.e., for the proper form of heat dissipation. In Model 1, the overall heat of reaction was divided between the two surface reactions: the one forming adsorbed CO and the other converting it to CO_2.

The resulting sets of coupled nonlinear ordinary differential equations were solved using the IMSL subroutine DGEAR. For any particular experiment, e.g., a TPR experiment, the simulation was begun by using the experimental initial conditions for the inlet concentrations and wall temperature. The initial conditions for the remaining dependent variables, such as those in the intraphase and on the surface, were obtained by performing the integration in time with no change in the inputs until steady-state conditions were reached. Thereafter, the experimental conditions were utilized in performing the simulation.

Results

Figure 1 shows the experimental data, together with their simulations, from a TPR experiment at 1% ethylene, 11% oxygen, and 180 cm^3/min nitrogen, on catalyst-B. Figure 1a shows the reactor wall temperature as it was raised and then lowered in a quasilinear fashion, as well as the simulated and experimental responses of the surface temperature. Experimentally, the surface temperature was measured at the inlet section and at the outlet section of the catalyst wafer, and both measurements are shown in the figure. The deviations between the two measurements occur primarily prior to extinction, with localized extinctions occurring at different wall temperatures. Recently, the source of reaction rate non-uniformities has been found to be related to non-uniformities in catalyst distribution and crystallite sizes (Sant and Wolf, 1987, 1988). As can be seen in Figure 1, nonuniformities become important during transitions between steady states, and the rate is spatially rather uniform when operating in either the high or the low steady state. The model involves no spatial dependence and the simulation of the surface temperature by Model 2 compares well with the experimental data only in the high and low steady states. Model 1 predicts an earlier extinction than either Model 2 or the experiment. However, the ignition temperature and the surface temperature rise at ignition, compare well with the other two cases (Model 2 and experiment). Similarly, Figure 1b shows the measured and simulated rates of CO_2 formation with deviations occurring primarily near extinction. This is a typical result wherein, experimentally, certain parts of the catalyst extinguish before other parts and hence, on lowering the wall temperature after ignition, the overall rate of CO_2 formation decreases gradually at first and then sharply during the final extinction. Our spatially uniform model can only predict a single sharp extinction.

By repeating the experiment as well as the simulations shown in Figure 1, at different values of the inlet ethylene concentration but keeping the same inlet oxygen flow rate, the cross-section of the bifurcation set was obtained. This cross-section is shown in Figure 3 for 11% oxygen and 180 cm^3/min nitrogen. The values of the kinetic and transport coefficients were

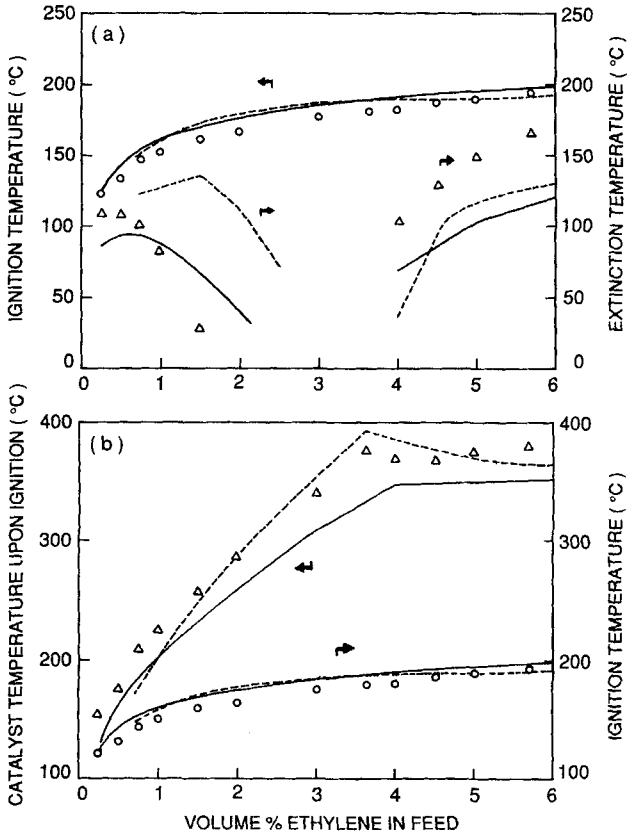

Figure 3. Experimental and simulated cross-sections of the bifurcation set showing (a) ignition and extinction temperatures, and (b) catalyst temperatures upon ignition, and ignition temperatures, at 23 cm^3/min oxygen and 180 cm^3/min nitrogen.

o, Δ, Experiment; – – –, Model 1; ——, Model 2.

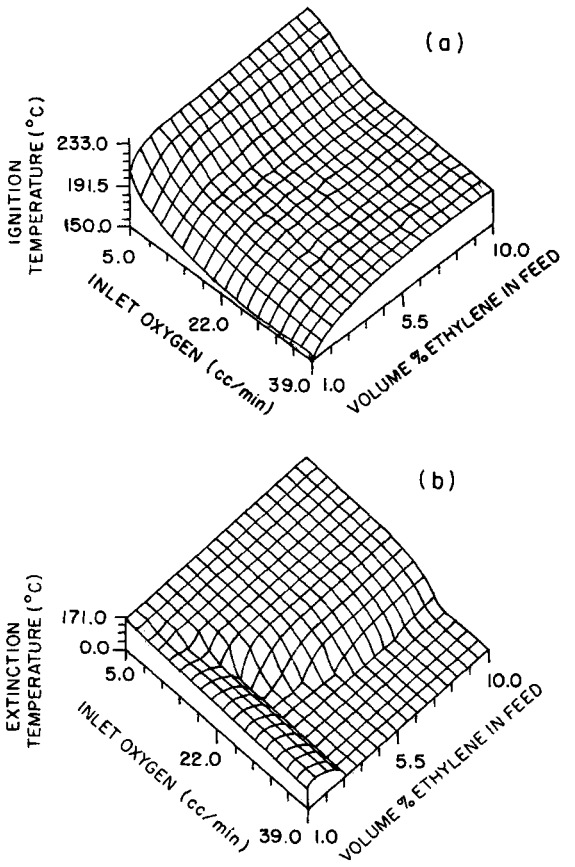

Figure 4. Three-dimensional bifurcation set simulated by Model 1 showing (a) ignition temperatures and (b) extinction temperatures.

adjusted within their experimentally-reported ranges (from the literature) so as to obtain the best possible match between the simulated and the experimental cross-sections of the bifurcation set. In Figure 3, the simulated cross-section from Model 2 is shown in continuous lines, that from Model 1 in dotted lines, and the experimental cross-section is shown as individual points. The experimental bifurcation points were obtained on catalyst B. The ignition and extinction points are shown in Figure 3a while Figure 3b shows the temperature of the surface upon ignition for the same values of inlet ethylene concentration as in Figure 3a. Once the parameters were fixed at the values used to obtain Figure 3, the ethylene and oxygen concentrations were varied systematically in order to simulate (via Models 1 and 2) the three-dimensional bifurcation set in the parameter space composed of gas temperature, inlet ethylene concentration and inlet oxygen flow rate. Figure 4a shows the ignition temperatures and Figure 4b shows the extinction temperatures for Model 1, while Figures 5a and 5b do the same for Model 2.

One can observe from Figure 3 that the ignition temperatures increase with increasing inlet ethylene concentrations, rapidly at first and more gradually once the stoichiometric ratio is exceeded. The extinction temperatures, on the other hand, are close to the ignition temperatures at very low and at very high ethylene concentrations. At intermediate concentrations of ethylene, the extinction temperatures decrease rapidly, occurring below room temperature for some concentrations. This description refers to the particular inlet flow rate of oxygen used in Figure 3. Figures 4 and 5 show, via simulation, how this behavior depends on the inlet concentration of oxygen. Thus, at low concentrations of inlet oxygen one observes primarily the no-hysteresis behavior, wherein the ethylene concentrations are high enough over most of the range to cause ignition and extinction to occur at virtually the same temperature. However, at high concentrations of inlet oxygen there is a steadily greater tendency for hysteresis until the high-ethylene branch of the extinction curve disappears entirely. In this regime, surface temperatures are too high to permit inhibition by ethylene (and hence the reaction does not extinguish even at room temperature).

A sensitivity analysis of kinetic and transport coefficients and the catalyst properties was carried out to examine the effects of changing each of these parameters by a small percentage of its standard value. The standard value of the parameters are those shown in Tables 3 and 4. The results of the sensitivity analysis were obtained in the form of the ensuing changes in ignition and extinction temperatures and, in some cases, in the form of changes in the surface–to–gas temperature difference and ethylene conversion just after ignition. These changes were calculated relative to a standard set of values obtained with the parameters at their standard levels. The standard set of ignition and extinction temperatures was that obtained for 2.1 cm^3/min ethylene, 23 cm^3/min oxygen, and 180 cm^3/min nitrogen (experimental and simulated results for these conditions are shown

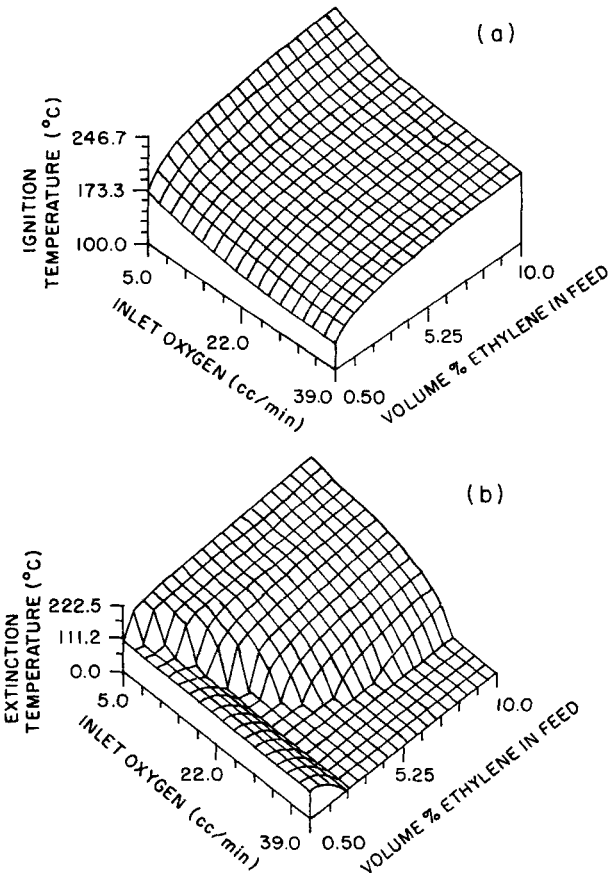

Figure 5. Three-dimensional bifurcation set simulated by Model 2 showing (a) ignition temperatures and (b) extinction temperatures.

Table 4. Values of Catalyst Properties and Transport Parameters

Parameter	Unit	Value	Source
a	m^2/m^3	1.3×10^6	Measured
N_s	mol/m^2	2.0×10^{-5}	Kaul et al. (1987)
A_s	m^2	5.67×10^{-4}	Kaul et al. (1987)
A_r	m^2	3.0×10^{-3}	Kaul et al. (1987)
ϵ_s	—	0.7	Measured
ρ_s	kg/m^3	7.0×10^2	Measured
V_r	m^3	6.0×10^{-6}	Kaul et al. (1987)
V_s	m^3	4.2×10^{-8}	Kaul et al. (1987)
h_s	$W/m^2/K$	29.26 (25.08)* (Model 1)	Kaul et al. (1987)
		37.62 (25.08)* (Model 2)	Kaul et al. (1987)
U_w	$W/m^2/K$	4.18×10^2	Kaul et al. (1987)
k_g	m/s	2.0×10^{-2}	Kaul et al. (1987)
C_{ps}	J/kg/K	1.00×10^3	Kaul et al. (1987)
C_{pg}	J/kg/K	1.05×10^3	Kaul et al. (1987)
ΔH_r (Model 2)	J/mol	1.32×10^6	Satterfield (1980)
ΔH_3 (Model 1)	J/mol	3.78×10^5	Calculated
ΔH_5 (Model 1)	J/mol	2.83×10^5	Kaul et al. (1987)

*Value used was increased from source value which is given in parentheses.

in Figure 1). Detailed results of the sensitivity analysis are available in the Supplementary Material and a summary is provided below.

In brief, the ignition temperature was very sensitive to changes in the activation energy for the desorption of ethylene and mildly sensitive to changes in the sticking coefficients of oxygen and ethylene respectively, as well as to changes in the preexponential factor to the desorption of ethylene. As far as the transport and catalyst parameters were concerned, the ignition temperature was primarily sensitive to changes in the active surface-to-volume ratio, a, of the catalyst and hence also to changes in the volume, V_s, of the catalyst. The extinction temperature was very sensitive to changes in the surface reaction parameters, $k_{0,3}$ and E_3, and to changes in the catalyst-to-gas heat transfer coefficient, h_s. Additionally, for Model 1, both ignition and extinction temperatures were strongly sensitive to the parameters for both surface reactions (formation of adsorbed CO and its conversion to CO_2), to the catalyst-to-gas heat transfer coefficient, as well as to the catalyst volume and to the active surface-to-volume ratio.

The results from the simulations help to explain how the combination of kinetic steps (adsorption, desorption and surface reaction) and transport processes (heat and mass transfer) can bring about the complex results that were observed in the experiments. For example, the experimental data and the simulations of an O_2-CPR experiment at 200°C are shown in Figure 6. Figures 6a and 6b show the rate of CO_2 formation and the catalyst surface temperature respectively, as the oxygen flow rate was ramped linearly up and then down. The experimental data have been taken from Kaul (1985) and these were obtained on catalyst A. Figures 6c and 6d depict the simulated surface coverages as functions of the surface temperature and the gas concentrations. Figure 6c, for Model 2, and Figure 6d, for Model 1, show that the roles of adsorbed ethylene and adsorbed CO in the respective models are roughly analogous. One can observe the inhibition effect of CO/ethylene (Model 1/Model 2) at low oxygen concentrations when the rate of oxygen adsorption in the rate-determining step. Once ignition occurs, the supply of reactants, primarily ethylene which now becomes the limiting reactant, from the bulk gas phase becomes the rate-limiting step.

Ethylene-CPR experiments performed at 160°C and at 200°C exhibit considerable differences as shown by Kaul and Wolf (1986) on catalyst A. The differences in behavior between the two temperatures can be understood by examining the simulated results at 150°C and at 200°C shown in Figures 7 and 8, respectively. As in Figure 6, Figures 7a and 8a depict the rates of CO_2 formation, and Figures 7b and 8b show the surface temperatures. These are done for the experimental data and for the simulations from Models 1 and 2. Figures 7c, 7d, 8c and 8d depict the simulated surface coverages for the respective experiments. Again, in Models 1 and 2, adsorbed CO and adsorbed ethylene can be seen to play analogous roles. At the lower temperature of 150°C, the rate of desorption of CO/ethylene (Model 1/Model 2) is sufficiently small as to cause the reaction to become extinguished once the concentration of ethylene becomes large enough. Thus the inhibition effect of CO/ethylene becomes strong enough to cause the surface to become covered primarily by CO/ethylene, with a resulting shortage of sites available for oxygen to adsorb onto and undergo reaction. At the higher temperature of 200°C, however, the rate of desorption of CO/ethylene is sufficiently large as to prevent the reaction from becoming extinguished altogether. Thus, although the simulations do not reproduce the experimental

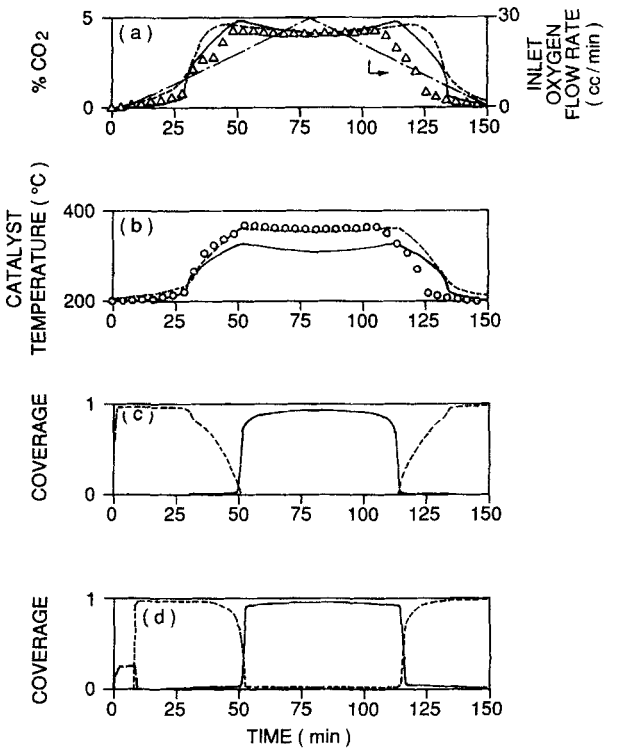

Figure 6. Experimental and simulated results of an oxygen-CPR experiment at 6 cm^3/min ethylene, 180 cm^3/min nitrogen, wall temperature = 200°C, and an O_2 ramp rate of 25 cm^3/min/h.

(a) CO_2 production rate; (b) catalyst surface temperature. Simulated responses of coverages are shown in (c) for Model 2, and (d) for Model 1. In (a) and (b): o, Δ, Experiment; — — —, Model 1; ———, Model 2; — · —, Ramp rate. In (c): ———, oxygen coverage; – – –, ethylene coverage. In (d): ———, oxygen coverage; – – –, CO coverage; — — —, ethylene coverage.

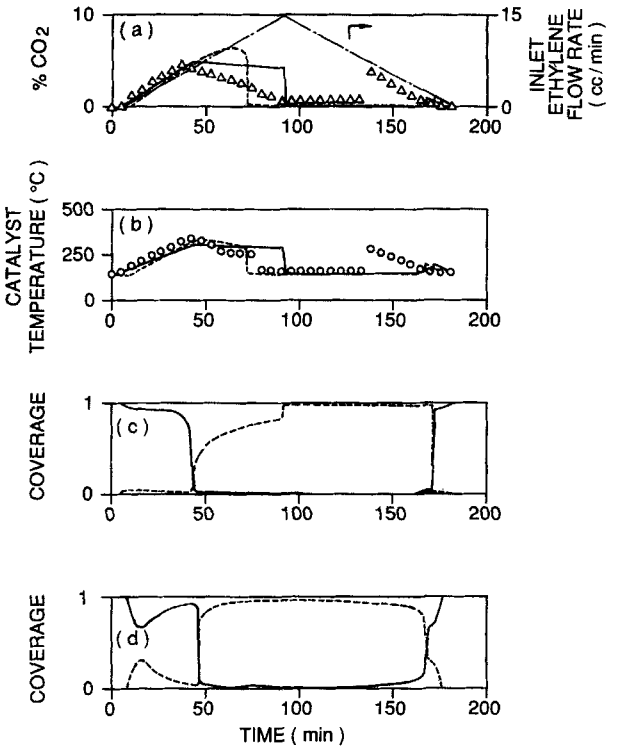

Figure 7. Experimental and simulated results of an ethylene-CPR experiment at 20 cm³/min oxygen, 180 cm³/min nitrogen, wall temperature = 160°C for the experiment and 150°C for the simulations, and an ethylene ramp rate of 10 cm³/min/h.

(a) CO_2 production rate, (b) catalyst surface temperature. Simulated responses of coverages are shown in (c) for Model 2, and (d) for Model 1. In (a) and (b): o, Δ, experiment; — — —, Model 1; ———, Model 2; — · —, Ramp rate. In (c): ———, oxygen coverage; – – –, ethylene coverage. In (d): ———, oxygen coverage; – – –, CO coverage; — — —, ethylene coverage.

results identically, they provide a rationale for explaining the behavior in terms of surface processes and gas-surface interactions.

Discussion

The Pt-catalyzed complete oxidation of ethylene is a complex reaction and the steps through which it proceeds have not yet been established clearly. In the past this reaction has been modeled either through a Langmuir-Hinshelwood rate expression in terms of global bulk variables (e.g., Paspek and Varma, 1980) or through an Eley-Rideal-type mechanism (e.g., Carberry, 1977). Vayenas et al. (1981) utilized a nonequilibrium kinetic model for this system. This model incorporated an Eley-Rideal pathway, and the oxidation of platinum. The emphasis was on simulating oscillatory behavior, rather than on the surface intermediates leading from ethylene to CO_2 formation. The present work assumes that the reaction proceeds through the following steps:

1) Adsorption, desorption and decomposition of ethylene and desorption of decomposition products

2) Adsorption and desorption of oxygen

3) Surface reactions between adsorbed species to form CO_2 and water

These assumptions were made primarily for two reasons. Firstly, studies on single crystals at UHV conditions have established that ethylene adsorbs on platinum, undergoes rearrangement and reacts with adsorbed oxygen to form carbon dioxide and water (Steininger et al., 1982; Berlowitz et al., 1985). Secondly, studies by Kaul and Wolf (1985a, 1986) and the studies described here indicate that the overall features of ethylene oxidation on Pt are similar to those of CO oxidation on Pt. These features include inhibition kinetics, reaction exothermicity, steady-state multiplicity and hysteresis, and regions of oscillatory behavior. Specifically, our studies (this work and that of Kaul et al. (1987)) as well as those of Zhukov and Barelko (1976) (for ethylene oxidation), and Harold and Luss (1985) (for CO oxidation), indicate that the dependence of the ignition and extinction temperatures on a bifurcation parameter such as the inlet ethylene or CO concentration (as the case may be), is primarily the same for both CO oxidation and ethylene oxidation on Pt.

The proper prediction of steady-state kinetics and hysteresis, steady-state multiplicity, and bifurcation from one steady state to another is an important first step towards understanding the mechanism of a reaction. Although it would be very desirable if periodic behavior could be predicted by a model, this was not the aim of the present work since, in our experiments oscillations

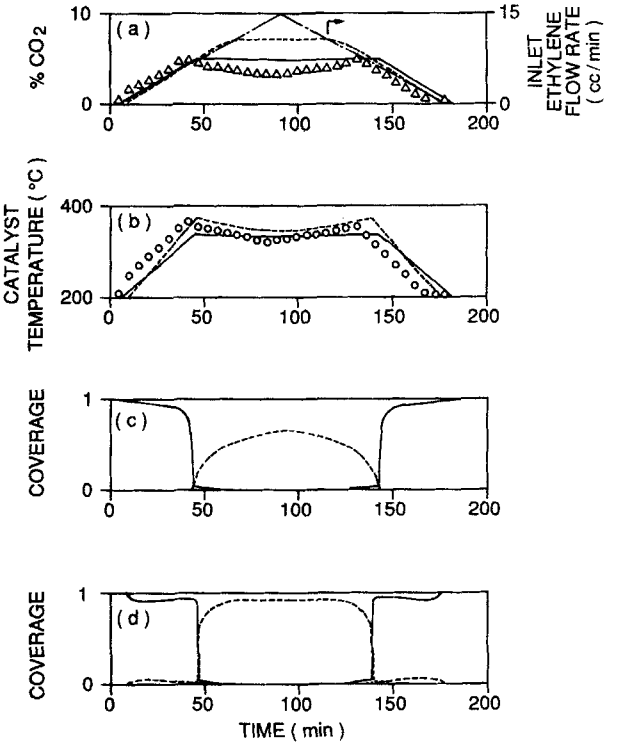

Figure 8. Experimental and simulated results of an ethylene-CPR experiment at 20 cm³/min oxygen, 180 cm³/min nitrogen, wall temperature = 200°C, and an ethylene ramp rate of 10 cm³/min/h.

(a) CO_2 production rate, (b) catalyst surface temperature. Simulated responses of coverages are shown in (c) for Model 2, and (d) Model 1. In (a) and (b): o, Δ, experiment; — — —, Model 1; ———, Model 2; — · —, Ramp rate. In (c): ———, oxygen coverage; – – –, ethylene coverage. In (d): ———, oxygen coverage; – – –, CO coverage; — — —, ethylene coverage.

occurred only over a certain subset of the entire parameter space and hence were the exception rather than the rule. Also, as described by Kaul and Wolf (1986), these time-varying states were found to be associated with spatial nonuniformities of various kinds. The model being described in this work, however, assumes spatially uniform concentrations and temperatures. Furthermore, it appears that the origin of oscillatory behavior lies in various kinds of surface transformations which remain to be clarified. In this connection, Vayenas et al. (1980, 1981) reported the oxidation of platinum (and its subsequent reduction) to be associated with rate oscillations. Our models do not predict oscillatory behavior without invoking a specific mechanism to do so. Our experimental results showed that oscillations occurred only in the ethylene-rich regime, when the surface is likely to remain reduced in the low and high conversion states, as well as in oscillatory states. Hence, it does not seem likely that an oxidation-reduction scheme is involved in our observations of oscillations for this system (Kaul and Wolf, 1986).

Berlowitz et al. (1985) reported a value of 5.73×10^4 J/mol for the activation energy of desorption of ethylene from an oxygen-covered Pt(111) surface, assuming a pre-exponential factor of 10^{13}. The values used in Model 2, however, are 1.15×10^5 J/mol and 6.5×10^{13}, respectively. This large difference, especially in the activation energy, can be understood, at least in part, by examining the species that are actually desorbing under various conditions. While the detailed pathway for the reaction has not been established, work done so far indicates that the reaction proceeds through one or more intermediates produced from the decomposition of adsorbed ethylene. A typical sequence of steps has been described in the section on theory. Hence, the elementary steps being used in Model 2 are at best an approximation to the actual pathway, with all the actual reaction intermediates being lumped into a species we denote as adsorbed ethylene. If the parameter values for ethylene desorption reported by Berlowitz et al. (1985) are used, the inhibition of oxygen adsorption by ethylene is absent, contrary to our experimental observations. Very significantly, the activation energy for ethylene desorption used in Model 2 is very similar to that for CO desorption. This further supports the conclusion that the inhibition effects more likely are caused by the decomposition products of adsorbed ethylene rather than by adsorbed ethylene itself. One of these decomposition products could well be adsorbed CO as shown in the infrared spectra of Figures 2a and 2b, and in the sequence of steps described in the section on theory. Quantitative evidence to support this claim is actually provided by Model 1, where the elementary rate constants for CO oxidation on Pt/SiO_2 (from Kaul et al., 1987) have been used without being altered in any manner. Moreover, Model 1 utilizes the ethylene desorption parameters as reported by Berlowitz et al. (1985). Thereafter, the best possible match between experiment and simulation was obtained for the adsorbed ethylene–to–adsorbed CO reaction described by a preexponential factor of 6.0×10^{13} and an activation energy of 6.27×10^4 J/mol, both of which appear to be reasonable and certainly are realistic. Hence, the present state of knowledge regarding the surface chemistry of the total oxidation of ethylene on Pt, as well as the parameter values and results of this study point to the conclusion that the role of the decomposition products and reaction intermediates from adsorbed ethylene is almost exactly analogous to the role of adsorbed CO in the oxidation of CO on Pt. It is worthwhile noting that McCabe and McCready (1984) have reported calculations from experiments indicating that adsorbed CO could be an intermediate in the oxidation of formaldehyde on a Pt wire catalyst.

The apparent lack of infrared data in the present study requires some clarification. As detailed by Kaul (1985), the IR bands for adsorbed ethylene were of weak intensity in the absence of reaction, and were completely obscured by other bands during reaction. Moreover, under oxygen-rich conditions there was a marked absence of IR bands for adsorbed species. The IR reactor in the present study was used earlier by Kaul and Wolf (1986) to show the occurrence of multiplicity, oscillations and spatial rate non-uniformities for this reaction system. While incorporating the surface chemistry, the aim in the present work was to simulate the steady-state portions and the ignition and extinction behavior of the experiments, some of which were described in the reference cited above. The objective here was to utilize the approach and results from our previous model for CO oxidation on Pt/SiO_2 (Kaul et al., (1987)) and relate those results to ethylene oxidation. This is especially true of Model 1, where the kinetic constants for CO oxidation were used directly from the reference just cited, without any changes. The use of the same IR reactor, then, permitted this comparison since the same reactor and catalyst configuration were maintained in both studies.

It must be pointed out that Model 1 does not match the experimental extinction data too well at very low ethylene concentrations (Figure 3) whereas Model 2 performs rather well. This is also borne out in the extinction behavior shown in Figure 1, wherein Model 1 predicts extinction to occur at a higher gas temperature than either the experiment or Model 2. In fact, in Figure 3a, Model 1 predicts the cusp point (separating the unique state region from the two-state region, and where the ignition and extinction curves coalesce) to occur at a higher value of the inlet ethylene concentration than either the experimental data or Model 2. This discrepancy could be related to the fact that the rate of CO adsorption is proportional to the first power of the concentration of vacant sites, θ_v, while the rate of ethylene adsorption is taken as being proportional to θ_v^2. Thus, the direct route from adsorbed ethylene to CO_2 production appears to be favored over the adsorbed CO intermediate route under oxygen-rich conditions. The adsorbed CO intermediate route, on the other hand, seems to become important under ethylene-rich conditions. This, however, only underscores the fact that there are several intermediates, including those leading to the formation of water, which have not been considered in the present work. However, it is rather significant that adsorbed CO can be shown, quantitatively, to be a possible route to CO_2 formation. Models 1 and 2, then, provide reasonable agreement between theory and experimental data over the majority of the conditions studied. Model 1 does not simulate the data well at very low ethylene concentrations, whereas Model 2 performs well at low ethylene concentrations but does not agree well with the experimental results at very high ethylene concentrations.

The three-dimensional bifurcation sets shown in Figures 4 and 5 depict concisely the dependence of the reaction behavior on gas temperature and ethylene and oxygen concentrations. One can quickly observe regions of wide hysteresis (high oxygen and high ethylene) as well as regions where the inhibition effects of ethylene are strong (low oxygen and high ethylene). Furthermore, the impact of the reaction exothermicity on the reaction behavior can be noted in the form of very low extinction temper-

atures even at intermediate oxygen and ethylene concentrations. The simulations of the O_2-CPR and ethylene-CPR experiments (Figures 6–8) illustrate how bulk observations can be interpreted in terms of surface coverages and temperatures as explained in the previous section. Figure 2 of Kaul and Wolf (1986) shows that the behavior of adsorbed CO is, indeed, qualitatively very similar to that predicted by Model 1. A quantitative comparison is difficult because, in reality, there are several adsorbed species in addition to adsorbed CO. The species which have been proposed include acetylene, ethylidyne, dehydrogenated acrolein, and others containing >C═O, >C═C< and —C—H groups. The sensitivity analyses indicate the specific rate processes and parameters that determine the ignition and extinction behavior. For example, in Model 1 the most significant parameters are those describing the two surface reactions: the first forming adsorbed CO, and the second converting it to CO_2. In Model 2, the ethylene desorption parameters strongly affect the ignition temperature, while the surface reaction parameters have a major impact on the extinction process. This is virtually identical to the results for CO oxidation on Pt/SiO_2 (Kaul et al., 1987), and further accentuates the similarities between these two reaction systems.

In order to understand the differences between the present elementary-step modeling approach and the older single rate-determining step concept, a comparison was made between the two approaches. Specifically, Model 1 was modified by assuming that the surface reaction between adsorbed CO and adsorbed oxygen was the rate-determining step. The other steps were then taken to be in equilibrium. The differential equations for the surface coverages were then replaced by algebraic expressions, details of which are provided in Appendix A. This modified model, denoted as the equilibrium model, was then used to perform the simulations of Figure 1. The results are shown in Figure 9, comparing the equilibrium model with the elementary-step models, 1 and 2. For clarity, the experimental data have not been shown, but they can be observed in Figure 1. Figure 9 shows that the equilibrium model predicts only the high conversion state for the TPR experiment, and hence predicts neither ignition nor extinction. Although not shown, the oxygen coverage remained high throughout the simulation by the equilibrium model (as necessitated by the assumption), which in turn, resulted in the high conversion state. While no claim is being made towards having obtained the true reaction pathway, it is hoped that this example will convey the advantages of the elementary-step modeling approach.

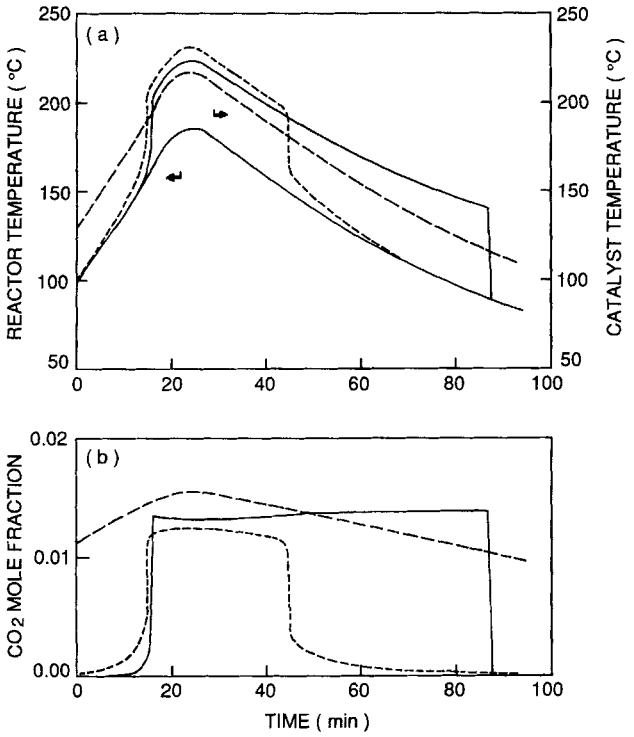

Figure 9. Simulated results of the TPR experiment depicted in Figure 1, comparing Model 1, Model 2 and the equilibrium model.

(a) Response of the catalyst surface temperature, (b) CO_2 production rate. – – –, Model 1; ——, Model 2; — — —, equilibrium model.

The results from this work provide an approach to a more complete understanding of the total oxidation of ethylene on Pt. It has been shown that the main experimental features can be explained via surface reactions between adsorbed oxygen and adsorbed ethylene and adsorbed intermediates derived from the latter. In describing the adsorption, desorption and reaction processes, as much information as possible has been utilized from studies at UHV conditions. An important conclusion to be drawn from the simulations is that it may no longer be necessary to think in terms of a single rate-determining step for this reaction, with other steps being in equilibrium. In fact, the drawbacks of this latter approach are illustrated in Figure 9. Instead, different steps occur simultaneously and, depending on the conditions that prevail at a given time, the rate-determining step can actually change, say from being O_2-adsorption-limited before ignition to being ethylene-supply-limited after ignition (for the experiments in Figures 1 and 6).

In conclusion, this paper provides a description and explanation of the steady-state multiplicity behavior of the ethylene oxidation reaction on Pt/SiO_2 catalysts. Qualitative and quantitative evidence have been provided to show how adsorbed intermediates like adsorbed ethylene and adsorbed CO can lead to the formation of CO_2. The specific intermediate(s) could depend on the operating conditions (e.g., ethylene-rich vs. oxygen-rich reactant mixtures). Experimental measurements of surface and bulk variables combined with simulations via a nonequilibrium elementary-step model provide insights into the origin and manifestation of steady-state multiplicity and hysteresis for this reaction. This has been done for oxygen-rich as well as ethylene-rich conditions. The construction of the cross-section of the bifurcation set, both experimental and simulated, provides a crucial means of linking experiments and theory. A variety of oscillatory and spatially non-uniform features have been shown in our previous work to occur during the oxidation of ethylene on Pt. Although such behavior cannot be described by the spatially uniform model, the results described here, together with those from our previous studies of CO oxidation on Pt, provide an avenue towards a more complete understanding of a general class of catalytic oxidation reactions.

Acknowledgment

Financial support of this research by the National Science Foundation through Grants CPE 84-5900 (equipment) and CBT-8603033 is gratefully acknowledged.

Notation

a = surface to volume ratio, m^2 Pt/m^3 catalyst
A_s = catalyst surface area, m^2
A_r = reactor wall surface area, m^2
C_g = bulk gas concentration, mol/m^3
C_s = intraphase gas concentration, mol/m^3
C_{pg} = heat capacity of feed gas mixture, J/kg/K
C_{ps} = heat capacity of porous catalyst particle, J/kg/K
E_i = activation energy for individual rate constants, J/mol
h_s = interphase catalyst heat transfer coefficient, W/m^2/K
ΔH_r = heat of reaction, J/mol
k_i = individual rate constant for adsorption (m^3/mol/s), desorption (s^{-1}) or surface reaction (s^{-1})
$k_{0,i}$ = preexponential factor for individual rate constants, units of k_i
k_g = interphase mass transfer coefficient, m/s
L = catalyst wafer thickness, m
M_i = individual molecular weights
N_s = number of active sites per unit active metal area, mol/m^2
Q = volumetric flow rate of feed gas mixture, m^3/s
R = gas constant, m^3 · atm/mol/K or J/mol/K
S_i = individual sticking coefficients
T_g = bulk gas temperature, K
T_s = catalyst surface temperature, K
T_w = reactor wall temperature, K
U_w = overall bulk gas-reactor wall heat coefficient, W/m^2/K
V_s = volume of catalyst wafer, m^3
V_r = volume of reactor, m^3
θ_i = fraction of sites covered with adsorbed species i
ϵ_s = porosity of catalyst wafer
ρ_g = density of bulk gas mixture, kg/m^3
ρ_s = density of porous catalyst wafer, kg/m^3

Subscript

i = 1–5 refer to oxygen, ethylene, carbon dioxide, carbon monoxide and water, respectively, except for θ_3, where subscript 3 refers to carbon monoxide

Literature Cited

Beebe, T. P., and J. T. Yates, Jr., "IR Spectroscopic Investigation of the Ethylene Chemisorption Reaction on Supported Metallic Catalyst Surfaces: Ethylidyne Formation on Pt, Rh, Pd and Ru Supported on Alumina," *J. Phys. Chem.*, **91,** 254 (1987).

Berlowitz, P., C. Megiris, J. B. Butt, and H. H. Kung, "Temperature-Programmed Desorption Study of Ethylene on a Clean, a H-Covered and an O-Covered Pt(111) Surface," *Langmuir*, **1,** 206 (1985).

Bertolini, J. C., and J. Massardier, "Hydrocarbons on Metals," *The Chemical Physics of Solid Surfaces and Heterogeneous Catalysis*, D. A. King and D. P. Woodruff, eds., **3B,** 107 (1984).

Cant, N. W., and W. K. Hall, "Catalytic Oxidation: II. Silica Supported Noble Metals for the Oxidation of Ethylene and Propylene," *J. Catal.*, **16,** 220 (1970).

Carberry, J. J., "Surface Activity in the Oxidation of Olefins on Deposited Pt," *Kinet. Kat.*, **18,** 562 (1977).

Fischer, T. E., and S. R. Kelemen, "Adsorption of Ethylene on the Pt(100) Surface," *Surface Sci.*, **69,** 485 (1977).

Gorte, R. J., and L. D. Schmidt, "Desorption Kinetics with Precursor Intermediates," *Surface Sci.*, **76,** 559 (1978).

Harold, M. P., and D. Luss, "An Experimental Study of Steady-State Multiplicity of Two Parallel Catalytic Reactions," *Chem. Eng. Sci.*, **40,** 39 (1985).

Hawkins, J. R., and S. E. Wanke, "The Oxidation of Ethylene over a Supported Pt Catalyst," *Can. J. Chem. Eng.*, **57,** 621 (1979).

Kaul, D. J., Ph.D. Thesis, Univ. of Notre Dame (1985).

Kaul, D. J., and E. E. Wolf, "FTIR Studies of Surface Reaction Dynamics: I. Temperature and Concentration Programming during CO Oxidation on Pt/SiO_2," *J. Cat.*, **89,** 348 (1984).

———, "FTIR Spectroscopy Studies of Surface Reaction Dynamics: II. Surface Coverage and Inhomogeneous Temperature Patterns of Self-Sustained Oscillations during CO oxidation on Pt/SiO_2," *J. Cat.*, **91,** 216 (1985a).

———, "Selected Area FTIR Studies of Surface Reaction Dynamics: III. Spatial Coverage and Temperature Patterns during Self-Sustained Oscillations of CO Oxidation on Pd/SiO_2," *J. Cat.*, **93,** 321 (1985b).

———, "Transient FTIR Studies of Multiplicities, Oscillations and Reaction Nonuniformities during CO and Ethylene Oxidation on Pt and Pd Catalysts," *Chem. Eng. Sci.*, **41,** 1101 (1986).

Kaul, D. J., R. Sant, and E. E. Wolf, "Integrated Kinetic Modelling and Transient FTIR Studies of CO Oxidation on Pt/SiO_2," *Chem. Eng. Sci.*, **42,** 1399 (1987).

McCabe, R. W., and D. F. McCready, "Formaldehyde Oxidation on Pt: Kinetic Evidence for Adsorbed Carbon Monoxide Intermediate," *Chem. Phys. Lett.*, **111,** 89 (1984).

Megiris, C. E., P. Berlowitz, J. B. Butt, and H. H. Kung, "Temperature-Programmed Desorption Study of C_2H_2 on a Clean, H-Covered, and O-Covered Pt(111) Surface," *Surface Sci.*, **159,** 184 (1985).

Palmer, R. L., "Molecular-Beam Study of Oxygen and C_2 Hydrocarbon Chemisorption and Reactions on Pt(111)," *J. Vac. Sci. Technol.*, **12,** 1403 (1975).

Paspek, S. C., and A. Varma, "An Experimental and Theoretical Investigation of Ethylene Oxidation on Supported Pt in an Adiabatic Fixed Bed Reactor," *Chem. Eng. Sci.*, **35,** 33 (1980).

Sant, R., and E. E. Wolf, "FTIR Studies of Spatial Effects of the Ignition Transition during the Oxidation of CO on Pt/SiO_2," *Surface Sci.*, **187,** 511 (1987).

———, "FTIR Studies of Catalyst Preparation Effects on Spatial Propagation of Oscillations during CO Oxidation on Pt/SiO_2," *J. Cat.*, **110,** 249 (1988).

Satterfield, C. N., *Heterogeneous Catalysis in Practice*, McGraw-Hill, New York (1980).

Steininger, H., H. Ibach, and S. Lehwald, "Surface Reactions of Ethylene and Oxygen on Pt(111)," *Surface Sci.*, **117,** 685 (1982).

Vayenas, C. G., B. Lee, and J. Michaels, "Kinetics, Limit Cycles and Mechanism of the Ethylene Oxidation on Pt," *J. Cat.*, **66,** 36 (1980).

Vayenas, C. G., C. Georgakis, J. Michaels, and J. Tormo, "The Role of PtO_x in the Isothermal Rate Oscillations of Ethylene Oxidation on Pt," *J. Cat.*, **67,** 348 (1981).

Wang, P.-K., C. P. Slichter, and J. H. Sinfelt, "Structures and Reactions of C_2H_4 Absorbed on Small Pt Clusters," *J. Phys. Chem.*, **89,** 3606 (1985).

Zhukov, S. A., and V. V. Barelko, "Uniqueness of Stationary States in a Catalyzer and Flickering in the Oxidation of Ethylene on Pt," *Dokl. Akad. Nauk. SSSR*, **229,** 655 (1976).

Manuscript received Apr. 18, 1988, and revision received Aug. 15, 1988.

See NAPS document no. 04635 for 5 pages of supplementary material. Order from NAPS c/o Microfiche Publications, P.O. Box 3513, Grand Central Station, New York, NY 10163. Remit in advance in U.S. funds only $7.75 for photocopies or $4.00 for microfiche. Outside the U.S. and Canada, add postage of $4.50 for the first 20 pages and $1.00 for each of 10 pages of material thereafter, $1.50 for microfiche postage.